

## BENCHMARKING BETWEEN TWO FINITE ELEMENT CODES FOR A STRUCTURAL INTEGRITY ASSESSMENT OF WELDED STRUCTURE

Jefri Draup<sup>1</sup>, Sutham Arun<sup>2</sup>, Van-Xuan Tran<sup>3</sup>

<sup>1</sup> Researcher, EDF Energy R&D UK Centre - Nuclear, UK

<sup>2</sup> Professor, Mechanical Engineering, University of Phayao, Thailand

<sup>3</sup> Modelling and Simulation Manager, EDF Energy R&D UK Centre - Nuclear, UK

### ABSTRACT

For linear elastic FE analysis, the pre-crack in the test specimen was represented by the sharp crack, whereas the notched crack with the notched radius of 100  $\mu\text{m}$  was used to represent the pre-crack in elastic plastic FE analysis. In both type of FE analysis, the residual stress was introduced into the weld section of FE model by an iterative technique. The results show that, for the linear elastic FE analysis without the presence of residual stresses, the values of  $J$  obtained from ABAQUS and  $G$  obtained from Code\_Aster are in good agreement with R6 solution and path independent. However, for the case with the presence of residual stresses, the  $J$  and  $G$  values become path dependent. For elastic-plastic FE analysis which the pre-crack of the test specimen was represented by notched crack, the values of  $G$  obtained from CodeAster agree well with  $J$  values obtained from Abaqus only in the region adjacent to the inner and outer surfaces. Outside these regions, the values of  $G$  obtained from Code\_Aster are higher than those obtain from Abaqus. In addition, the two values are path dependent for the case with and without residual stresses.

### INTRODUCTION

This paper aims to evaluate and cross-validate the formulations of two fracture mechanics parameters, i.e. J-integral ( $J$ ) and the energy release rate ( $G$ ) using ABAQUS and Code\_Aster, an open-source finite element software developed by EDF R&D since 1989 and devoted to structural analyses. The evaluation and validation were performed via a 3D finite element model of large scale four-point bending test (MU2-test) undertaken as part of STYLE Framework 7 project. A large-scale four point bending test performed by CEA (Bourgeois, 2014). The test specimen, referred to as MU-2, is a welded pipe consisting of two lengths of Esshete 1250 austenitic stainless steel joined by a girth weld. The weld contains a short, deep weld repair, and a through thickness pre-crack was introduced at the center of the repair. The main section of MU2 and the pre-crack position are schematically shown in Figure 1 and Figure 2, respectively.

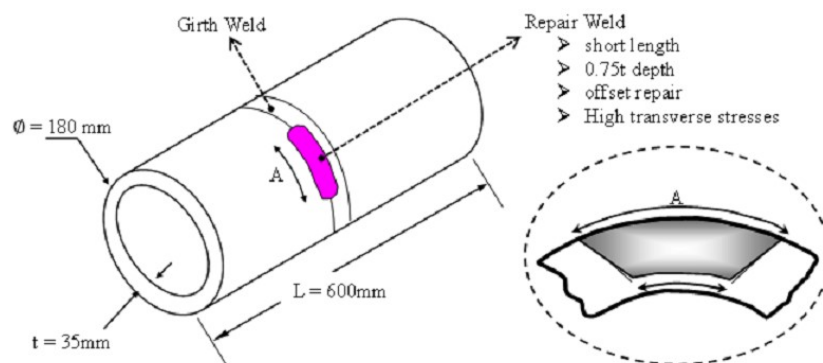


Figure 1. Schematic of MU2 pipe.

The MU2 pipe has overall dimensions of 600 mm length, 180 mm outer diameter and 35 mm wall thickness. Both ends of the specimen are joined to extension arms, which are manufactured from 304L stainless steel, to provide a 5 m four point bending span for the four-point bending experiment (Figure 4). The total length of the full test specimen is about 7.4m. The distance between the inner loading points is 1 m and between the outer loading points is 5 m. The experimental set-up is illustrated in Figure 3. The geometry input in the simulation is shown in Figure 5.

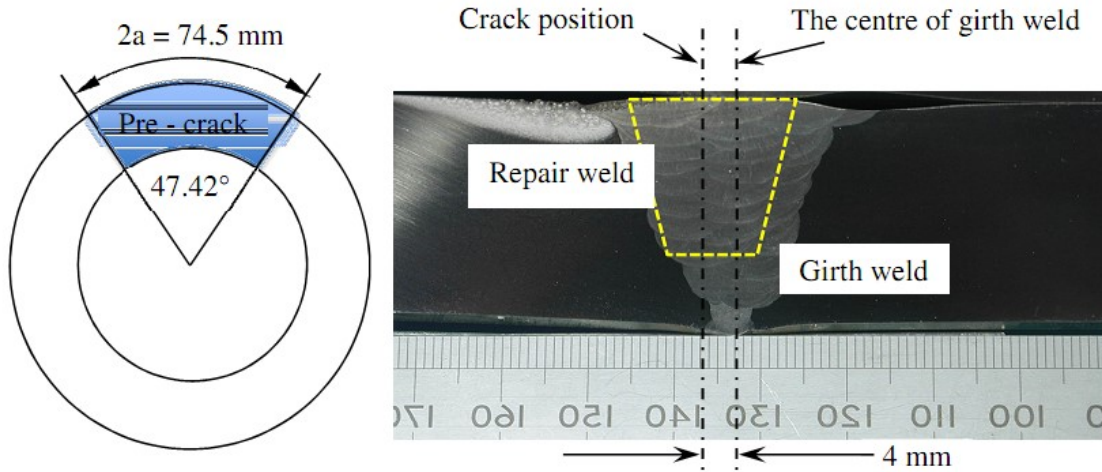


Figure 2. Dimensions of the through thickness pre-crack.

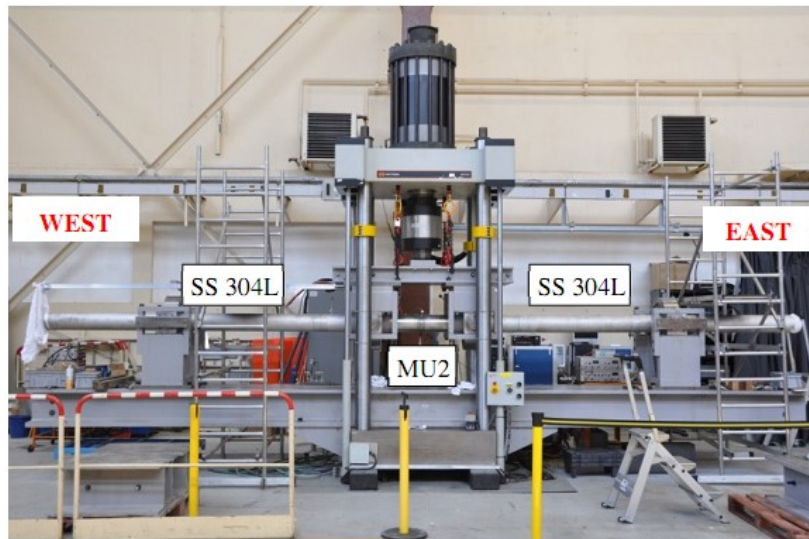


Figure 3. Set up for the large-scale four point bending experiment.

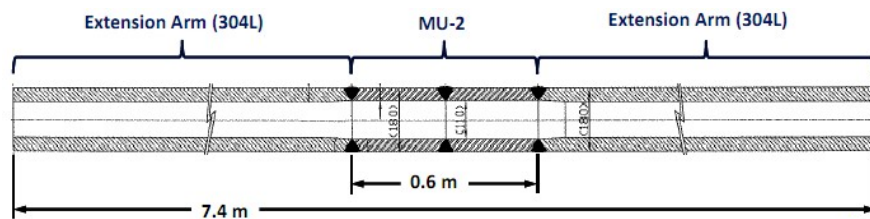


Figure 4. Full test specimen.

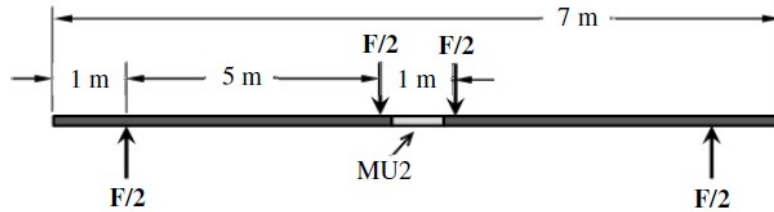


Figure 5. Geometry model

In the experimental framework, the experiment was divided into two main phases: a pre-cracking test and ductile tearing test. This work concerns the first phase pre-cracking test. The dimensions and shape of pre-crack is shown in Figure 6. To design the pre-crack, a V-shaped slot was introduced into the middle plane of the repair weld by electro-discharge machining prior to loading. The inserted crack is not at the center of specimen. The distance between crack position and the center of girth weld is 4 mm. Two crack fronts converge to the center of pipe and make an angle of  $47.42^\circ$  (Figure 2).

During the test, two clip gauges were attached at the outer surface of the pipe in order to measure the values of crack mouth opening displacement (CMOD) as show in Figure 6.

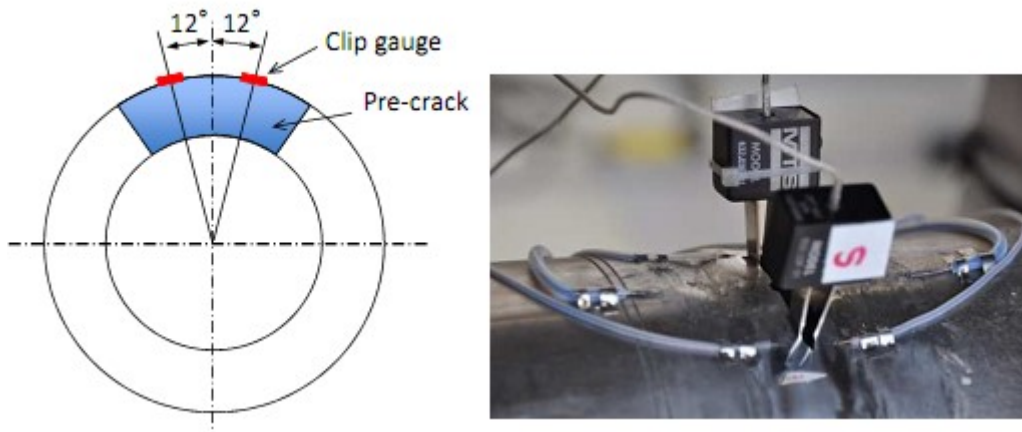


Figure 6. CMOD measurement position

Due to the symmetry of geometry and loading, one half of the full test specimen (MU2 and Extension arm) was modelled, thus the symmetry condition were applied on the symmetry surface.

## COMPUTATIONAL MODEL

### *Meshes*

Three linear meshes are employed in this study. The difference between them is in the crack type and the elements around crack tip:

- Mesh 1: sharp crack and unstructured mesh around crack tip ;
- Mesh 2: sharp crack and radiating mesh around crack tip;
- Mesh 3: notched crack 200 $\mu$ m of radius and radiating mesh around crack tip.

The element size around the crack tip is 0.1 mm for mesh 3 and 0.014 mm for mesh 2. 100 $\mu$ m radius on a notched crack represents both the crack tip radius in reality and a reasonable level of refinement mesh around crack tip in numerical simulation.

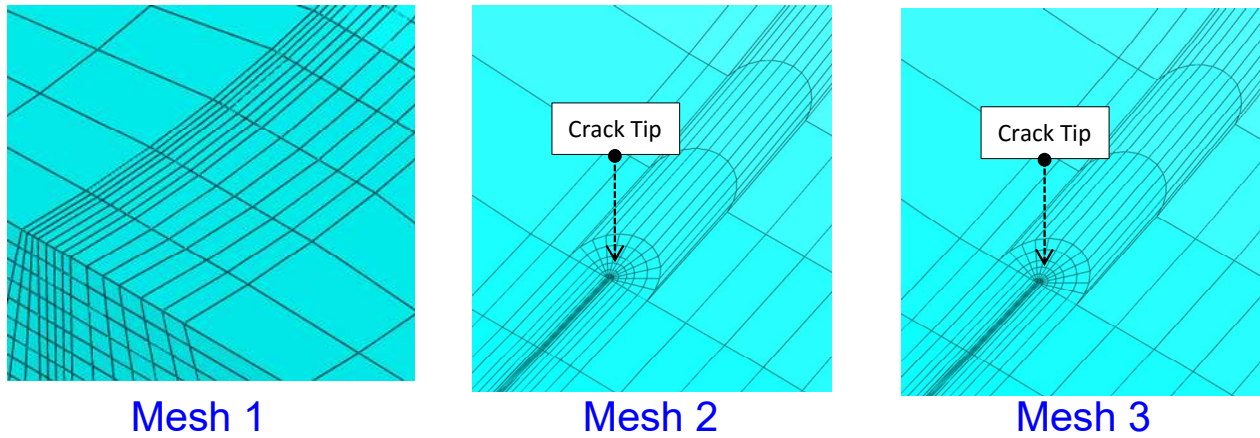


Figure 7. Three different meshes used in this study

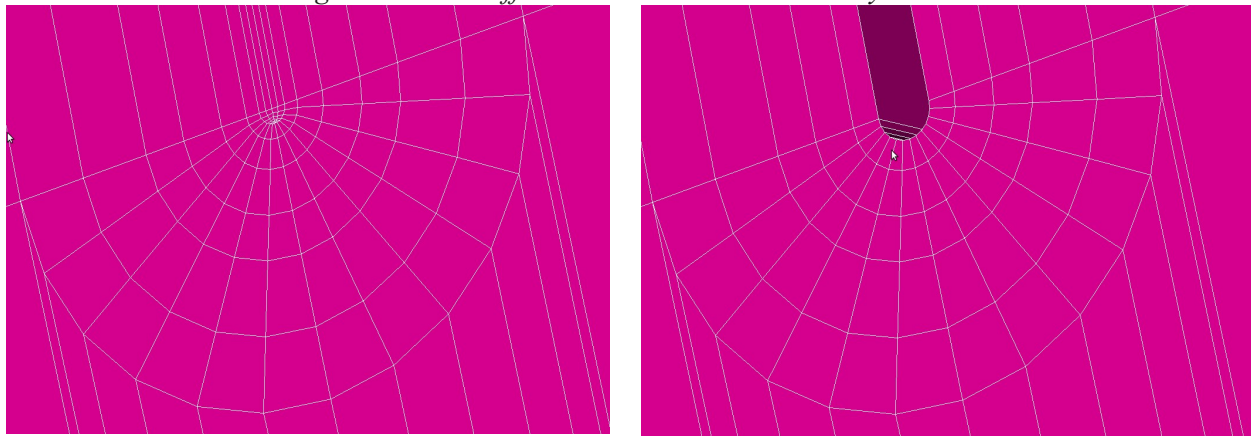
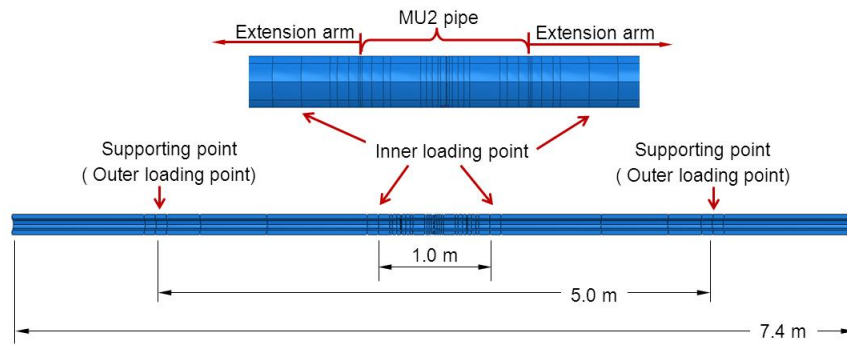


Figure 8. Different between mesh 2 and mesh 3.

### Boundary and loading conditions

The boundary and loading conditions are shown in Figure 9 where the supporting points, loading points, symmetry plane, and fixed points to prevent rigid body movement is defined. The distance between the supporting points is 5.0 m and between loading points is 1.0 m. For the supporting points, all translations and rotations are prevented, with the exception of rotation around the z-axis. The same constraints are applied to the loading points but with an applied downward vertical displacement. The latter constraint is applied at a single point on the outside surface of MU2 section, opposite to the crack location to prevent movement in axial direction of the structure.



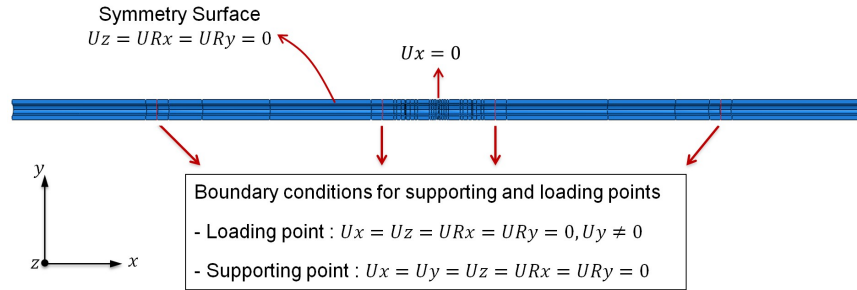


Figure 9. Boundary condition and loading

### Material properties

The tensile test data for as-received parent metal and weld metal were used for the Esshete stainless steel. As the data for the 304L extension piece and the extension weld materials for the test were not available, the material properties for 316L were used instead. The elastic properties of these four materials can be found in Table 1.

Material	E (GPa)	$\nu$
Esshete Parent	204.5	0.294
Esshete Weld	157.6	0.3
A316L Parent	195.6	0.294
A316L Weld	171.0	0.294

Table 1: Elastic properties of materials (Austin and Hayes, 2007; Blandford et ail., 2007)

For elastic-plastic simulation, the true stress/strain data for these four materials is presented in Figure 10. These curves allow modelling elastic-plastic materials as non-linear elastic one by using Hencky-Von Mises law.

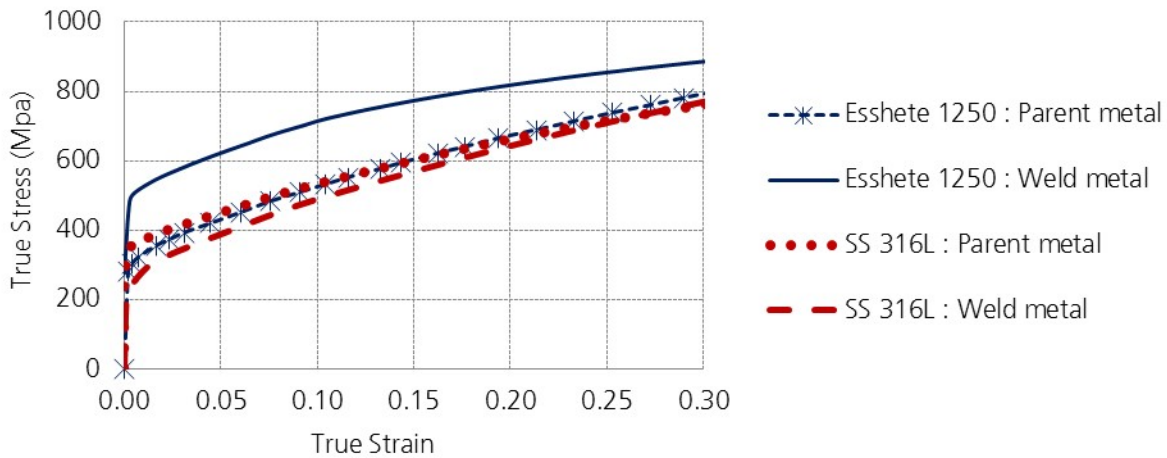


Figure 10. True stress/strain curves for elastic-plastic simulation

### Input of residual stresses

The measured residual stress data for weld Esshete pipe were given in large scale four point bending test simulation by Do and Smith (2014). These values were obtained from the application of the deep hole-technique described by Do et al. (2012). Figure 11 illustrates two lines of residual stress measurement, one along the center line of the repair weld and through the pipe wall thickness, and a second directly opposite to center repair well. In both cases, only the in-plane (i.e. hoop and axial) residual stresses were measured using incremental deep hole drilling.

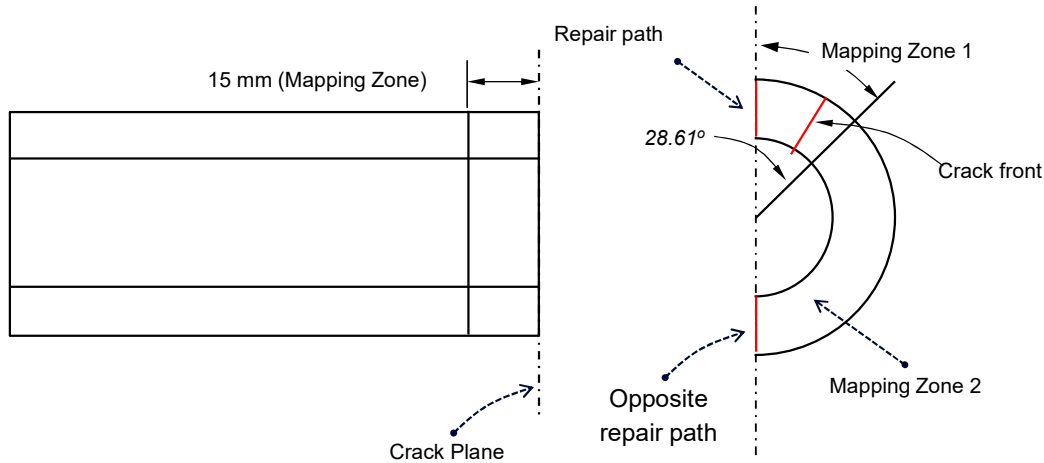


Figure 11. The location of two lines of residual stress measurement and mapping zones for the FE model.

The residual stress was introduced into the FE model of the full test specimen, but without the presence of crack. Two mapping zones for the repair weld and the remainder of original weld were defined according to the recommendation of Do and Smith (2014). These are shown in Figure 11. Mapping zone 1 was used to map the residual stresses obtained from the repair part, whereas the stresses measured from opposite repair path were imposed to mapping zone 2. This process was applied by assuming that the stresses along the measuring line were the same everywhere within the mapping zone.

Since the residual stress field introduced directly into FE model is always in non-equilibrium state, an equilibrium calculation (static computation with no additional load applied) was performed in order to obtain a self-equilibrated distribution of residual stress before applying loads to FE model. This step results in a difference between initial input stress and the obtained equilibrium residual stress. To minimize the error, an iterative method proposed by Lei et al. (2000) was used to transform the initial non-equilibrium residual stress to equilibrium one. This method is expressed by the following equation:

$$[\sigma]_{input}^{i+1} = [\sigma]_{input}^i + \alpha([\sigma]_{measured} - [\sigma]_{output}^i) \quad (1)$$

where  $[\sigma]_{input}$  is the initial stress input into FE model;  $[\sigma]_{measured}$  is the measured residual stress;  $[\sigma]_{output}$  is the resultant residual stress obtained after an equilibrium step. The superscript  $i$  means the  $i^{\text{th}}$  adjustment step and  $\alpha$  is an adjustment factor. The procedure starts with  $i=0$  and  $[\sigma]_{input} = [\sigma]_{measured}$  introduced in FE mode to obtain  $[\sigma]_{output}$ . The  $[\sigma]_{input}$  for the next iteration is calculated by Eq. (1). This procedure was repeated until an agreement between  $[\sigma]_{output}$  and  $[\sigma]_{measured}$  was obtained.

Figure 12 presents the self-equilibrium residual stress profiles obtained by iterative technique. After mapping process, the residual stress introduced on FE model along the repair path agree to within 5% of the measured values, in both axial and hoop components.

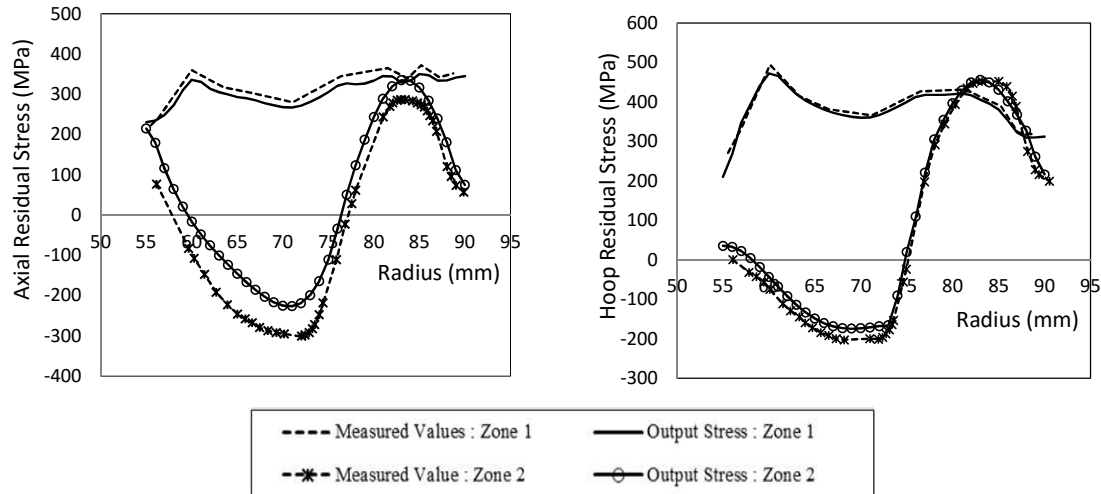


Figure 12. The measured residual stress and their corresponding self-equilibrium values from FE model

The equilibrium residual stresses were then mapped onto the cracked model for subsequent simulation with loading. The presence of crack again lead to a redistribution of residual stresses and a high stress value ahead the crack tip.

### COMPUTATIONAL RESULTS

This section synthetizes the energy release rates obtained by Code\_Aster and ABAQUS. As a reminder,  $G$  in Code\_Aster computed by G-theta method (CALC\_G operator with default smoothing method with torus of  $RI=0.0010$  m and  $RS=0.0015$  m), while  $J$  is obtained by J-integral in ABAQUS. Figure 14 recapitulates the variation of  $G/J$  at the middle crack versus the distance from the notch front.

These figures show that:

- $G$  and  $J$  are path-independent in elastic simulations without residual stress but both of them are path-dependency in elastic-plastic simulations;
- $G$  is path-independent while  $J$  is path-dependent in elastic simulations with residual stress;
- $G$  and  $J$  are in a perfect agreement in elastic simulations without residual stress;
- $G$  and  $J$  are in a good agreement in elastic simulations with residual stress due to the Path-independence of  $J$  in ABAQUS when adding an extra term in  $J$  formulation;
- The difference between  $G$  and  $J$  is more observable for elastic-plastic simulation with or without ( $\sim 13\%$  of relative different between  $G_{max}$  and  $J_{max}$ ). This difference may be due to the path-dependency of  $G$  and  $J$  in plastic behaviour.

The path-dependency of  $G/J$  in plastic material is an interesting subject that requires further depth in the formulations and numerical implementation of the G-theta method as well as J-integral. This research topic and is out of scope of this project.

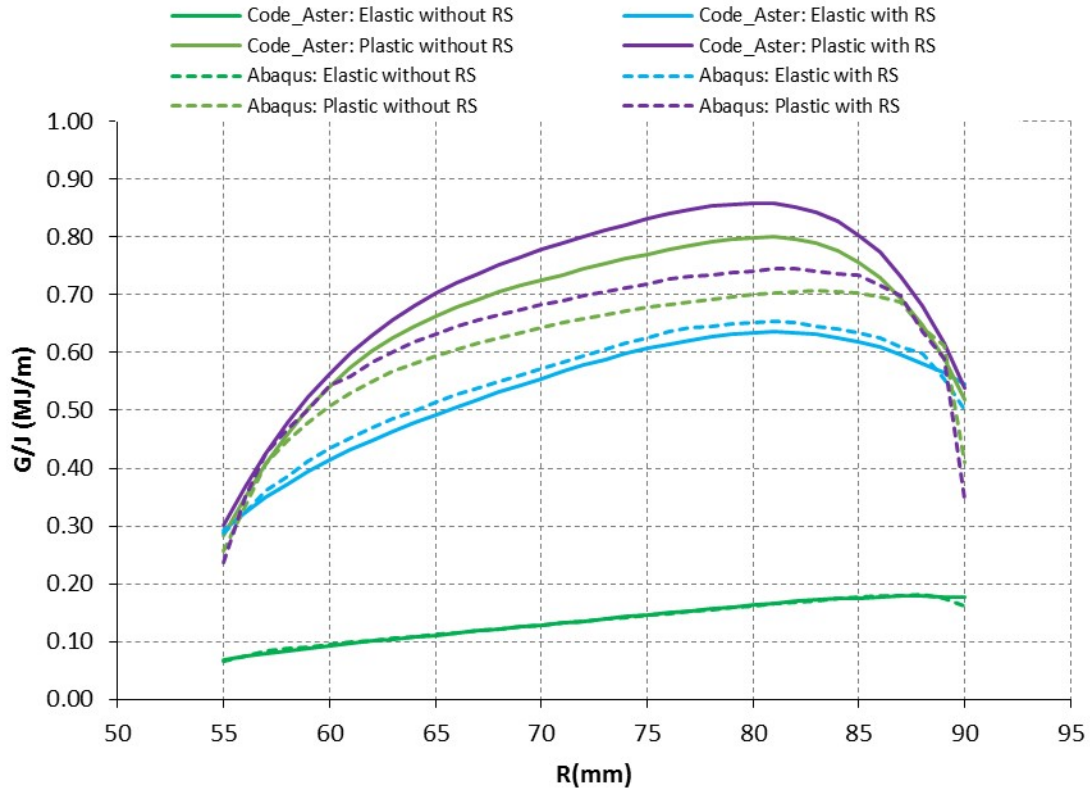


Figure 13. Comparison of Code\_Aster/ABAQUS.

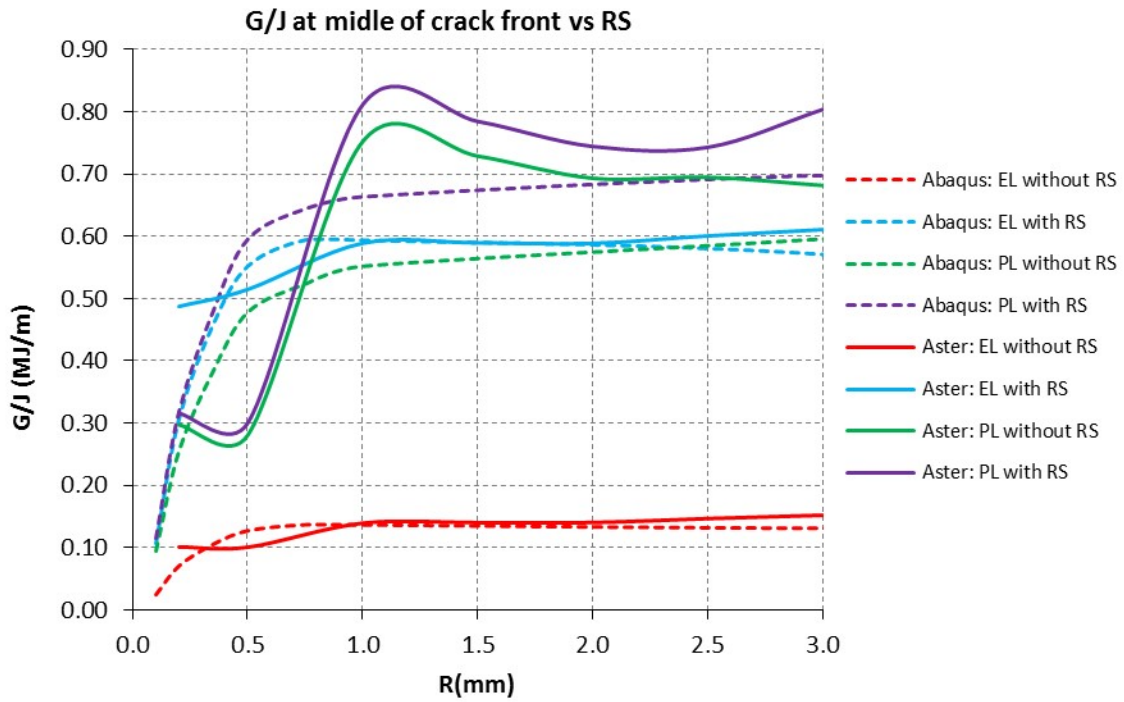


Figure 14. Variation of  $G/J$  at the middle of crack front versus distance from crack front

As presented in the previous figures, the following observations can be made:

- G is stable for elastic material both with and without residual stresses. In the thermo-elastic framework, G formulation implemented in Code\_Aster includes elementary term of elastic energy density; body force term; thermal term and initial stress or strain term.
- J obtained by ABAQUS exhibits path-independency only for elastic without residual stress case. J becomes path dependent unless an extra term for initial stresses is added (Moes et al., 2002; Muscati and Lee, 1994; Siegele, 1989). J-integral calculation has worked with initial stress from Abaqus version 6.11. Converged values of G along the crack obtained by G-theta method in Code\_Aster agree to J obtained by ABAQUS,
- Path-dependency of G and J for elastic-plastic material (with or without residual stress).

Theoretically, the G in elastic simulation is path-independent according to the G-theta method. This point has been numerically demonstrated by several test cases in Code\_Aster. However, elastic-plastic materials exhibit path-dependency. As a matter of fact, the limitation of G results from the assumed existence of a strain energy density, as a potential from which stresses can be uniquely derived. The assumption actually does not describe irreversible plastic deformation, as in the incremental theory of plasticity of VON MISES, PRANDTL and REUSS, but hyper-elastic or non-linear elastic behavior. It does not only exclude any local unloading processes but also any local re-arrangement of local stress, i.e. changing of loading direction in the stress space, resulting from yield condition. Moreover, an assumption of the calculations is that all loading paths in the stress space are supposed to remain radial so that the ratios of principal stresses do not change with time. The condition of monotonous global loading of a structure is of course not sufficient to guarantee radial stress paths in non-homogeneous stress fields. Hence, the G and J-integral will become path-dependent as soon as plasticity occurs and the torus and contour passes the plastic zone.

A residual stress field is a self-balancing stress distribution in a body. As mentioned above, such stresses can result from internal strains, due to, for example, non-uniform plastic deformation, non-uniform heat expansion or local volume change during phase transformation. If the internal strain field results in an additional mechanical strain field (without external loading), residual stresses are set up in the body. Such residual stress problems can then be treated as initial strain problem. Based on this analyse, Lei et al. (2002) proposed a path independent J definition for a crack in a residual stress field. A good path independence of the modified J was shown by analysing a number of crack geometries containing residual stresses using finite element method. This modified J formulation is not yet available in Code\_Aster nor in Abaqus standard. A numerical implementation of this formulation through Macro-command in Code\_Aster seems to be not difficult.

## CONCLUSIONS

For linear elastic FE analysis, the pre-crack in the test specimen was represented by the sharp crack, whereas the notched crack with the notched radius of 100 Pm was used to represent the pre-crack in elastic plastic FE analysis. In both type of FE analysis, the residual stress was introduced into the weld section of FE model by an iterative technique. The results show that, for the linear elastic FE analysis without the presence of residual stresses, the values of J obtained from ABAQUS and G obtained from Code\_Aster are in good agreement with R6 solution and path independent. However, for the case with the presence of residual stresses, the J and G values become path dependent. For elastic-plastic FE analysis which the pre-crack of the test specimen was represented by notched crack, the values of G obtained from CodeAster agree well with J values obtained from Abaqus only in the region adjacent to the inner and outer surfaces. Outside these regions, the values of G obtained from Code\_Aster are higher than those obtain from Abaqus. In addition, the two values are path dependent for the case with and without residual stresses.

## REFERENCES

- Austin C., Hayes J.P., (2007) A Constitutive Model for Parent Esshete 1250 and Associated Single Bead Weld Metal. Serco Assurance Report SA/SIA/17261/R01, SERCO, UK,2005.
- Blandford R.K., Morton D.K., Snow S.D., Rahl T.E. (2007), Tensile stress-strain results for 304L and 316L stainless steel plate at temperature. Proceedings of the ASME 2007 Pressure Vessels & Piping Conference, Texas, USA, 2007.
- Bourgeois (2014) M., Mock-Up 2 Test. STYLE report D-1.15, 2014, CEA, France.
- Do S., Smith D.J. (2014), Simulations of a Large-scale Four Point Bending Experiment; Influence of Residual Stresses from a Repair Weld. Procedia Materials Science, 2014, vol.3 (0),pp. 1599-1605.
- Do S., Smith D.J., Smith M.C. (2012), Effect of ageing on residual stresses in welded stainless steel cylinders. Proceedings of the ASME 2012 Pressure Vessels & Piping Conference, Toronto, Canada.
- Lei Y., O'Dowd N.P., Webster G.A. (2000), Fracture mechanics analysis of a crack in a residual stress field. International Journal of Fracture, 2000, vol.106 (3): 195-216.
- Moës N., Gravouil A., Belytschko T., (2002), Non-planar 3D crack growth by the extended finite element and level sets Part I: Mechanical model. International Journal for Numerical Methods in Engineering, 2002, 53: 2549-2568.
- Muscati, A., Lee, D.J., (1984), Elastic-plastic finite element analysis of thermally loaded cracked structures. Int. J. Fracture, Vol. 25: 2276-246.
- Siegele, D. (1989), 3D crack propagation using ADIN. Computers & Structures, 1989, 32: 639-645